Materials Science Forum
ISSN: 1662-9752, Vol. 1191, pp 55-60
doi:10.4028/p-4kesV3

Submitted: 2025-09-11
Revised: 2025-12-23
Accepted: 2026-03-16
Online: 2026-05-19

Edge Termination Design for Ultra High-Voltage (>10 kV) 4H-SiC Power Devices Using Background Doping Modulation (BDM)

Mohamed Torky[1,a*], Justin Lynch[1,b], Nick Yun[1,c], Stephen Mancini[1,d], Miguel Hinojosa[2,e], Aivars Lelis[2,f] and Woongje Sung[1,g]

[1]Department of Nanoscale Science and Engineering, University at Albany, Albany, NY 12203, U.S.A

[2]U.S. Army Research Laboratory (ARL), Adelphi, MD 20783 U.S.A

[a*]mtorky@albany.edu, [b]jmlynch@albany.edu, [c]nyun@albany.edu, [d]smancini@albany.edu, [e]miguel.hinojosa4.civ@army.mil, [f]aivars.j.lelis.civ@mail.mil, [g]wsung@albany.edu

Keywords: ultra-high-voltage, ion implantation, lateral straggle, TCAD simulation, edge termination techniques.

Abstract. Achieving reliable breakdown in ultra-high-voltage (>10 kV) SiC devices is limited by edge termination design, where low epitaxial doping (~4×10^{14} cm^{-3}) results in lateral straggle to be more prominent, therefore necessitating wider spacing between Aluminum implants in conventional floating field rings (FFRs). This study introduces a background doping modulation (BDM) scheme, incorporating a moderately doped N-type confinement region within P+ rings, enabling tighter spacing without added process complexity for high-voltage MOSFETs. Fabricated BDM-FFRs achieved >13 kV breakdown (30% higher than conventional FFRs), with leakage current <10 nA at 10 kV, while reducing termination area by 18.6%. Therefore, the BDM-FFR demonstrates a scalable, and high-performance edge termination approach for next-generation ultra-high-voltage SiC devices.

Introduction

Wide bandgap semiconductors such as silicon carbide (4H-SiC) have emerged as the most promising candidates for next-generation high-voltage and high-efficiency power devices. The materials' superior material properties, wide bandgap, high critical electric field, and excellent thermal conductivity enable devices capable of blocking voltages beyond 10 kV while operating with reduced conduction and switching losses. Such performance is critical for high-voltage direct current (HVDC) transmission, traction inverters, grid integration of renewable energy, and pulsed power systems [1]. Despite significant progress in device fabrication, the realization of reliable and reproducible breakdown voltages (BV) in ultra-high-voltage (>10 kV) devices remains challenging. A major limitation is the design of edge termination structures, which must suppress electric field crowding at the active area to achieve close-to-theoretical breakdown performance [2]. Conventional termination schemes—including floating field rings [3], junction termination extension (JTE) [4], and a hybrid combination of both designs [5] are widely adopted. In ultra-high-voltage SiC devices, the drift layer is typically thick (>100 μm) and lightly doped (~4×10^{14} cm^{-3}), which strongly impacts edge termination design. The low doping makes the lateral dopant straggle more prominent, degrading electric field control in conventional FFR structures and requiring wider ring spacing. To accommodate lateral and vertical depletion, the termination width must generally exceed five times the epi thickness, making it a dominant factor in total chip size. A proposed background doping modulation (BDM) ensures a reduced edge termination design that can significantly minimize the lateral straggle, reducing the chip size and hence the chip cost, through improving the blocking characteristics with small spacings.

Edge Termination Theory and Background

The ideal breakdown voltage of a one-dimensional p-n junction is determined by the peak electric field within the device, influenced by drift layer thickness and doping. Once the peak electric field

reaches the critical electric field of SiC, avalanche breakdown occurs. However, in real devices, field crowding at the active area limits the actual breakdown to ~70–80% of the theoretical value. To mitigate this, edge termination structures are implemented to spread the depletion region laterally and smooth out the electric field distribution. Among various approaches, floating field rings (FFRs) are particularly attractive for high-voltage applications due to their simplicity, scalability, and compatibility with both diode and MOSFET structures. They consist of multiple concentric P+ implanted rings surrounding the active region. The rings gradually drop the potential from the active junction edge to the device periphery, thereby reducing the peak field. However, the effectiveness of FFRs depends critically on ring spacing and dopant profiles, which are strongly influenced by the low doped background.

In 4H-SiC with very low background doping, implanted dopants undergo significant lateral diffusion and straggle [6]. This smearing of ring edges compromises the field distribution and requires increased spacing between rings (≥1 μm). For devices with a hundred rings, this can cause the termination width to extend to nearly 1 mm, which is prohibitive for compact high-current devices. Furthermore, too-small spacing can lead to premature breakdown due to field crowding at ring corners, while too-large spacing results in incomplete field modulation and premature breakdown due to field crowding at the cylindrical junction in the active area [2].

In 10 kV-class SiC devices, edge terminations can occupy ~80% of chip area for a 1 A-rated device and ~50% for a 10 A-rated device, as shown in Fig. 1, reducing current density, increasing cost per ampere, and limiting scalability. To address these issues, this work proposes a novel approach by adding N-type doping within the FFR structure, resulting in background doping modulation (BDM-FFR). By intentionally pre-doping a moderately N-type region before the implantation of the floating field rings, the lateral straggle is suppressed, enabling tighter ring spacing without field crowding [7]. This results in more compact termination, higher breakdown voltage, and reduced leakage current compared to conventional FFR designs.

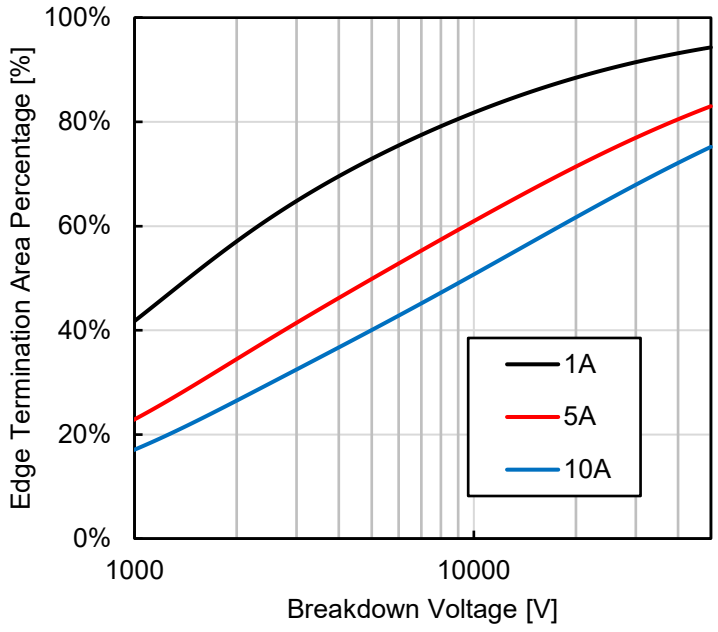

Fig. 1. Edge termination percentage as a function of breakdown voltage for different current ratings.

Fig. 2 and 3 show the structural differences between the conventional and proposed FFRs. It should be noted that the proposed BDM-FFRs do not require high energy implantation as the primary goal is to accomplish narrow spacing design between P+ concentric rings without increasing the electric field at their corners. Notably, this additional N-type implantation can coincide with the JFET region in standard MOSFET process flows, allowing seamless integration of the proposed structure without adding process complexity. In the case of Schottky or JBS diodes, however, an additional implantation step would be required.

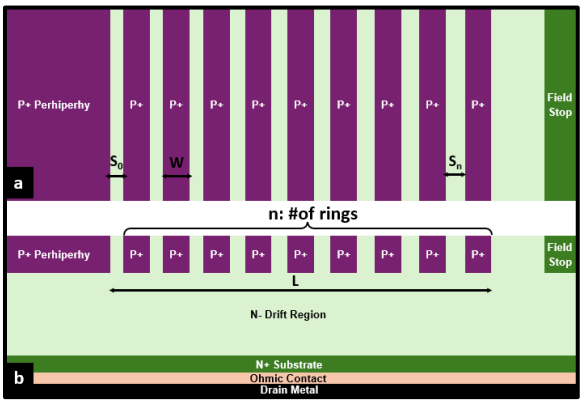

Fig. 2. (a) Top and (b) cross-sectional views of conventional FFRs.

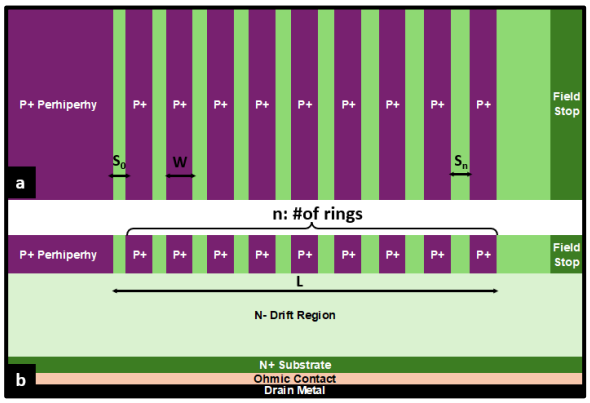

Fig. 3. (a) Top and (b) cross-sectional views of the proposed BDM-FFRs.

Edge Termination Fabrication

PiN diodes with three different edge terminations designs were fabricated on a 6-inch wafer with a drift layer thickness of 125 µm and N-type doping concentration of 4×10^{14} cm^{-3} enabling >10 kV blocking capabilities. Nitrogen implantation was used for implanting the background doping modulation (BDM) layer, while high temperature aluminum and nitrogen implantation was used for the P+ rings and the channel stop as shown in Fig. 2 and 3. After implantation, dopants are activated thermally at 1605 °C for 10 min. with a carbon cap. Three different edge termination designs were fabricated; one PiN diode has BDM-FFR with a ring width of 5 µm and a spacing of 0.8 µm. The other two PiN diodes have a conventional FFR design with a ring width of 3 µm and a spacing of 1 µm and 1.5 µm respectively to account for the lateral straggle due to the low doped background.

Table 1. Structural parameters for BDM-FFR, FFR1 and FFR2 devices.

Structural Parameters	BDM-FFR	FFR 1	FFR 2
BDM	Yes	No	No
W [µm]	5	3	3
S_0 [µm]	0.8	1	1.5
S_i [µm]	0.03	0.1	0.05
n	100	100	120
L [µm]	728.5	895	897

Table 1 illustrates the structural parameters for BDM-FFR and the two conventional FFRs. The n^{th} spacing between rings as a function of ring number is given by,

$$S_n = S_0 + (n+1)\,S_i \tag{1}$$

where S_0 is the initial spacing, n is the number of rings and S_i is the spacing increment. Fig. 4 illustrates the simulated doping profiles of both the BDM (N-type) and P+ rings where the BDM doping is a $2x10^{16}$ cm^{-3} box profile.

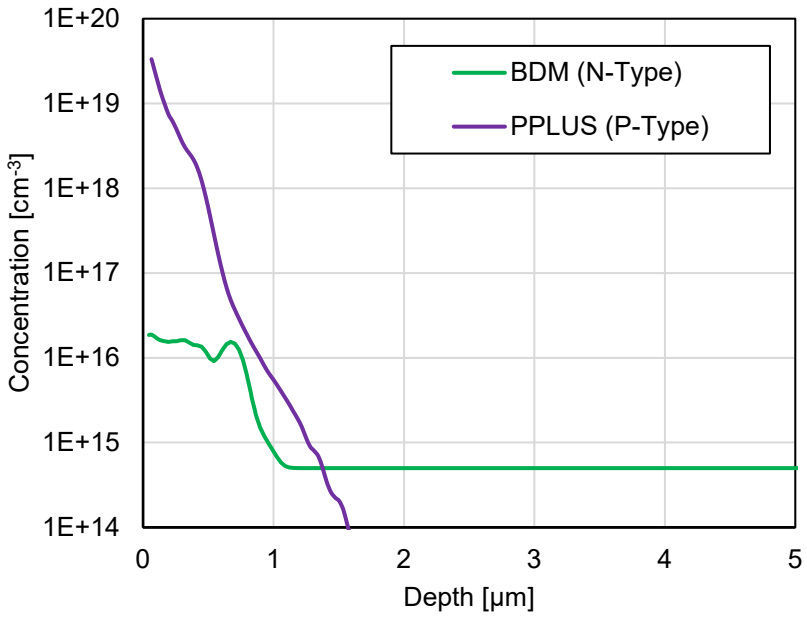

Fig. 4. BDM (N-type) and P+ implantation profiles used in our study from Sentaurus TCAD simulation.

Results and Discussion

As shown in Fig. 5 (a) and (b), cross-sectional imaging using Focused Ion Beam (FIB) and SEM confirmed the effectiveness of BDM with a minimal lateral straggle. BDM-FFR rings exhibit sharp boundaries with negligible lateral straggle even at increased depth, while conventional FFRs suffer from substantial smearing and overlap between adjacent rings. Conventional FFRs suffer from lateral straggle with 43% increase in the P+ width, which has been validated by TCAD simulation as shown in Fig. 6. Consequently, we designed the spacings of the conventional FFRs as illustrated in Table 1 to account for the lateral straggle at the expense of the edge termination width.

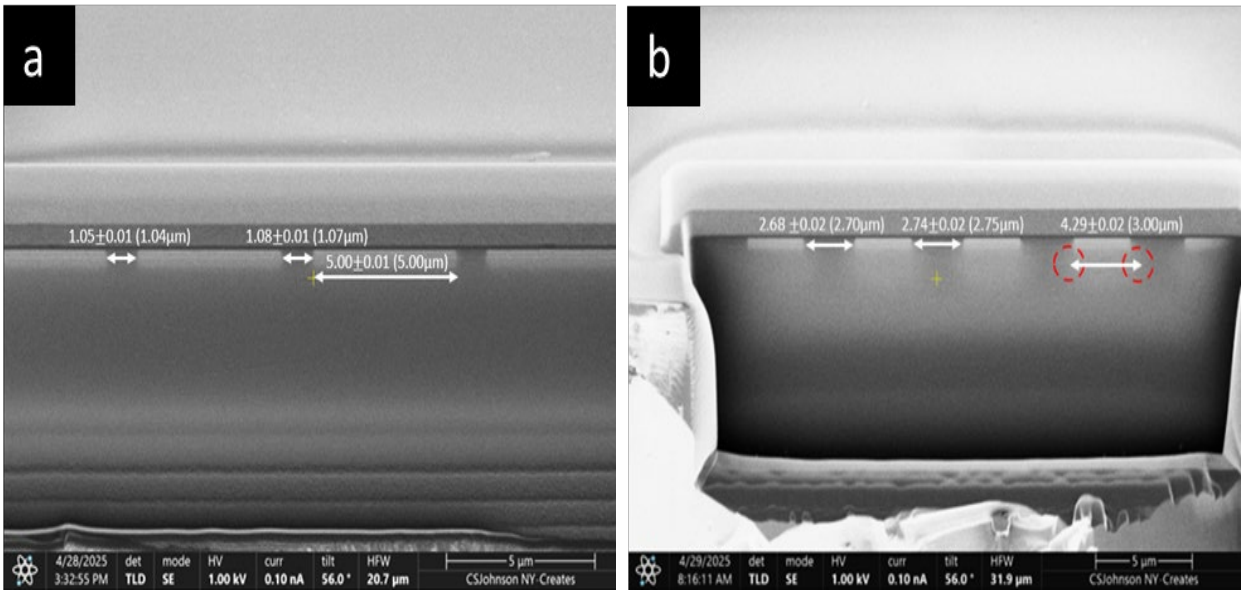

Fig. 5. SEM FIB cross-sectional view for (a) BDM-FFR and (b) conventional FFRs. Numbers inside parentheses denote the designed spacings.

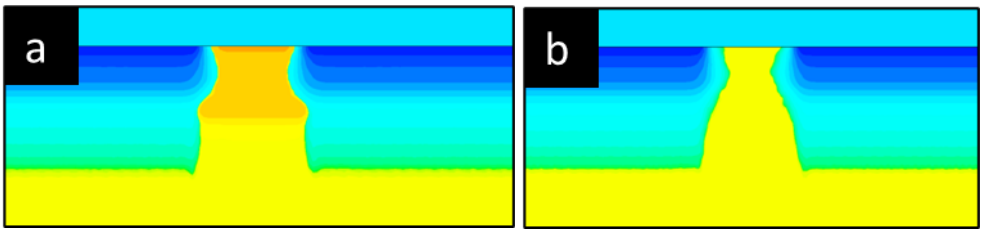

Fig. 6. Sentaurus simulation cross-sectional schematic showing the lateral straggle between (a) BDM-FFR and (b) conventional FFRs.

Wafer-level electrical characterization was performed using Keithley high-voltage probe stations. The breakdown voltage was defined at a leakage current of 100 µA, and leakage characteristics were measured up to 10 kV. Fig. 7 shows the blocking characteristics of FFR1, FFR2, and BDM-FFR. The BDM-FFR achieved a blocking voltage of 12.5 kV, approximately 24% higher than conventional FFR devices, which have a breakdown voltage of 10 and 10.7 kV, respectively. These results demonstrate the improved field control and reduced corner crowding afforded by the BDM-FFR technology, as it has wider rings and controlled spacings between rings due to the minimized lateral straggle. At 10 kV, BDM-FFR exhibited leakage currents of only 2 nA, three orders of magnitude lower than FFR1, which has a leakage current of 8 µA, and a 91% lower leakage in the case of FFR2, which has a leakage of 23 nA. The high leakage in FFR1 is attributed to insufficient ring separation (1 µm), leading to premature conduction and leakage paths. Although the P+ ring width of the BDM-FFR is 5 µm compared to conventional FFRs, the termination length (L) of BDM-FFR is only 728.5 µm, compared to ~895 µm for conventional FFRs, an 18.6% total area reduction. This reduction in total area is crucial for scaling to high-current devices where chip area directly impacts cost and manufacturability. The confinement layer limits lateral dopant struggle, thereby stabilizing potential distribution across the rings. This enables narrow ring spacing without excessive electric field concentration at ring corners, leading to higher BV and lower leakage. Table 2 shows the blocking characteristics for the three devices.

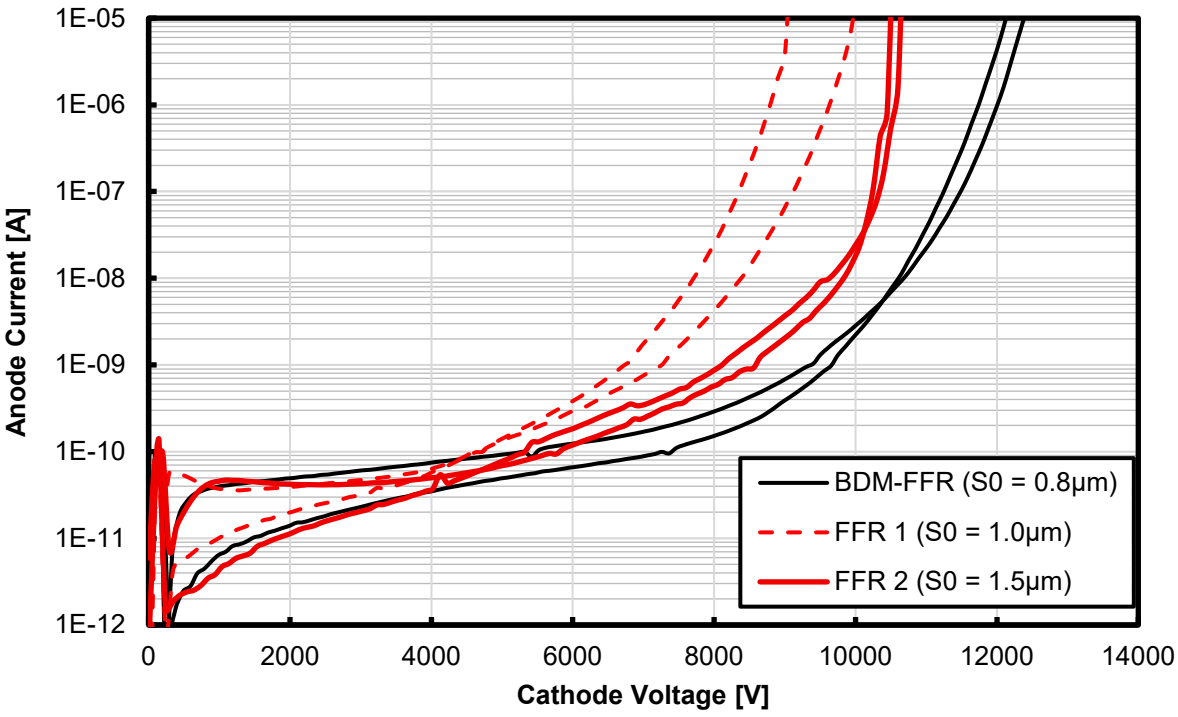

Fig. 7. Blocking characteristics of BDM-FFR, FFR 1 and FFR 2.

Table 2. Blocking voltage and leakage current for BDM-FFR, FFR1 and FFR2.

Blocking Performance	BDM-FFR (S_0 = 0.8 μm)	FFR 1 (S_0 = 1.0 μm)	FFR 2 (S_0 = 1.5 μm)
BV @ $I_{AK} = 10^{-5}$ A [V]	12.5	10	10.7
I_{DSS} @ V_{DS} = 10 kV [A]	2×10^{-9}	8.1×10^{-6}	2.3×10^{-8}

Conclusion

This work demonstrates a novel background doping modulation (BDM) edge termination for ultra-high-voltage (>10 kV) 4H-SiC power devices. By introducing a confinement layer beneath P+ floating field rings, lateral straggle is suppressed, enabling tighter designs with tight ring spacing. Compared to conventional FFRs, BDM-FFR achieved a breakdown voltage of 12.5 kV (24% improvement), leakage currents < 10 nA at 10 kV, and termination width reduction of ~18.6%. These results provide clear evidence that BDM offers a scalable, manufacturable, and high-performance solution for edge termination in next generation SiC power devices. Future work will extend this approach to devices beyond 15 kV and explore integration in power modules for high-current applications.

Acknowledgement

The authors would like to thank ADI for fabricating the devices. We also would like to thank Alexander Bialy and Cobert Johnson from NY CREATES for helping in taking FIB and SEM images in Fig. 5.

References

[1] J.B. Casady, R.W. Johnson, Status of silicon carbide (SiC) as a wide-bandgap semiconductor for high-temperature applications: A review, Solid-State Electronics 39 (10) (1996) 1409-1422.

[2] B. J. Baliga, Fundamentals of Power Semiconductor Devices. New York, NY, USA: Springer, 2008, Chap. 3, pp. 91–162.

[3] M.S. Adler, V.A.K. Temple, A. P. Ferro, R. C. Ruslay, Theory and breakdown voltage for planar devices with a single field limiting ring, IEEE Transaction on Electron Devices, 24 (2) (1977). 107-113.

[4] W. Sung, E. V. Brunt, B. J. Baliga, A. Q. Huang, A New Edge Termination Technique for High-Voltage Devices in 4H-SiC–Multiple-Floating-Zone Junction Termination Extension, IEEE Transaction on Electron Devices, 32 (7) (2011) 880-882.

[5] W. Sung, B. J. Baliga, A Near Ideal Edge Termination Technique for 4500V 4H-SiC Devices: the Hybrid Junction Termination Extension (Hybrid-JTE), IEEE Transaction on Electron Devices, 37 (12) (2016) 1609-1612.

[6] J. Lynch, N. Yun, W. Sung, Design Considerations for High Voltage SiC Power Devices: An Experimental Investigation into Channel Pinching of 10kV SiC Junction Barrier Schottky (JBS) Diodes, 31st International Symposium on Power Semiconductor Devices and ICs (ISPSD), Shanghai, China, (2019) 223-226.

[7] N. Yun, D. Kim, J. Lynch, A. J. Morgan, W. Sung, M. Kang, A. Agarwal, R. Green, A. Lelis, Developing 13-kV 4H-SiC MOSFETs: Significance of Implant Straggle, Channel Design, and MOS Process on Static Performance, IEEE Transaction on Electron Devices, 67 (10) (2020) 4346-4353.